Can a photometric redshift code reliably determine dust extinction?

T. S. R. Babbedge,[1]★ R. Whitaker[2]★ and S. Morris[2]★†

[1]*Astrophysics Group, Blackett Laboratory, Imperial College London, Prince Consort Road, London SW7 2BW*
[2]*Astronomy and Astrophysics, Physics Department, South Road, Durham DH1 3LE*

ABSTRACT

Photometric redshifts can be routinely obtained to accuracies of better than 0.1 in $\Delta z/(1 + z)$. The issue of dust extinction, however, is one that has still not been well quantified. In this paper the success of two template-fitting photometric redshift codes (ImpZ and hyperz) at reliably returning A_V in addition to redshift is explored. New data on the 2nd Canadian Network for Observational Cosmology (CNOC2) spectroscopic sample of $0.2 < z < 0.7$ galaxies are presented. These data allow us to estimate A_V values from the observed Balmer decrements. We also investigate whether the empirical value of $\gamma = 0.44$, the ratio between gas- and star-derived extinction, as determined by Calzetti, is necessarily the best value for this sample.

When comparing the two codes with the Balmer-derived A_V (Balmer[A_V]), a correlation between the photometrically derived A_V (Phot[A_V]) and the Balmer[A_V] is found. The correlation is improved when the empirical value of $\gamma = 0.44$ is allowed to vary. From least-squares fitting, the minimum in the reduced χ^2 distribution is found for $\gamma \sim 0.25 \pm 0.2$. For the sample of galaxies here, the factor of 2 difference in covering factor implied by the Calzetti ratio is found to be plausible. The CNOC2 galaxies with detected Balmer lines have some preference for an increased covering-factor difference, which perhaps implies that they are undergoing more rapid, 'bursty' star formation than the galaxies Calzetti used in her derivation.

Key words: galaxies: evolution – galaxies: photometry – quasars: general – cosmology: observations.

1 INTRODUCTION

Star formation rates (SFRs) and their global history (SFH) form the backbone of a slew of methods (observational, numerical, and analytical) investigating the processes of galaxy formation and evolution over cosmic time. The SFH is important in indicating likely eras of dominant activity and in providing a self-consistent picture of chemical enrichment. This can then be compared with the predictions of semi-analytical models of galaxy formation and with intergalactic medium (IGM) absorption-line diagnostics. However, SFRs can be imprecise as a result of complications arising from dust extinction.

COBE measurements of the cosmic far-infrared/submillimetre background energy density (Puget et al. 1996) showed it to be equal to, or greater than, the ultraviolet/optical background (e.g. Hauser et al. 1998), implying that a large fraction of the energy from stars over the history of the Universe is hidden in the optical as a result of dust. The role of dust in high-redshift galaxies has been discussed by

many authors (e.g. Rowan-Robinson et al. 1997; Pettini et al. 1998; Calzetti & Heckman 1999; Adelberger & Steidel 2000). For example, star-forming galaxies detected via the Lyman-break technique at $z \sim 2$–4 are estimated to be highly extincted in the rest-frame ultraviolet (UV), meaning star formation rates are $\sim$3–10 times higher than if dust is ignored (e.g. Meurer, Heckman & Calzetti 1999). Correction factors found for other high-redshift star-forming galaxies are of a similar order. The exact form of this extinction correction remains uncertain, and in particular so does its evolution with epoch.

Hence an important improvement for optical-based SFH studies is the determination of the extinction of galaxies, in addition to their redshifts. In order to allow fully for variation from galaxy to galaxy, extinction needs to be measured as an additional free parameter to redshift. The study of Bolzonella, Miralles & Pelló (2000), however, found that the inclusion of A_V as a free parameter in photometric redshift codes caused significant increases in aliasing. In a similar technique developed in Rowan-Robinson (2003), hereafter RR03, and extended in Babbedge et al. (2004), hereafter B04, these aliasing problems were reduced by setting several A_V priors.

In this paper a sample of galaxies from the 2nd Canadian Network for Observational Cosmology (CNOC2) Field Galaxy Redshift Survey (Yee et al. 2000) is used to investigate the reliability of A_V values as determined by two SED template-fitting photometric

★E-mail: tsb1@imperial.ac.uk (TSRB); r.j.whitaker@durham.ac.uk (RW); Simon.Morris@durham.ac.uk (SM)
†Visiting Astronomer, Canada–France–Hawaii Telescope.

Table 1. 5σ limits (Vega) for the four CNOC2 areas, and the Galactic extinction $E(B - V)$ in each area. This can be converted to a correction in each band via the method in Cardelli, Clayton & Mathis (1989) with $R_V = 3.1$.

Area	I_C	R_C	V	B	U	$E(B - V)$
0223	22.97	24.02	23.95	24.55	22.98	0.036
1447	23.52	23.72	24.35	24.76	23.27	0.029
0920	22.85	24.03	23.94	24.55	23.18	0.012
2148	22.69	23.88	23.70	24.48	23.08	0.035

redshift codes – HYPERZ (Bolzonella et al. 2000) and IMPZ (see B04) – by comparing the returned [z_{phot}, A_V] with the spectroscopically derived redshifts and Balmer-decrement-derived A_V values as calculated from CFHT MOS spectroscopic data.

In Section 2 the CNOC2 galaxy sample is set out, along with the follow-up CFHT spectroscopic data and Balmer-decrement calculations. In Section 3 we discuss the link between Balmer extinction and photometry. The photometric redshift method is briefly outlined in Section 4, and the results of applying the two redshift codes to the CNOC2 sample are presented in Section 5. Overall discussions and conclusions are presented in Section 6.

Note that for these investigations the flat $\Omega_\Lambda = 0.70$ cosmological model with $H_0 = 72\,\mathrm{km\,s^{-1}\,Mpc^{-1}}$ is used.

2 CNOC2 OVERVIEW

The CNOC2 survey was conducted over a series of 53 nights on the Canada–France–Hawaii Telescope from 1995 to 1998 (Yee et al. 2000). The survey covers a total area of 1.5 deg^2 spread over four patches equally spaced in RA. The data set includes $\sim$6000 galaxy spectra with spectroscopic redshifts to a nominal limit of $R_C \sim 21.5$ in addition to five-colour (I_C, R_C, V, B, U)[1] photometry of 40 000 galaxies, complete to $R_C = 23.0$ mag. The mean limiting magnitudes (Vega, 5σ) in each filter for the four areas are given in Table 1, and the filter response curves are shown in Fig. 1.

Use of a band-limiting filter restricted the spectral window in the survey to 4400–6300 Å. This includes the [O II] emission line for redshifts between 0.18 and 0.69. The survey's results on galaxy clustering over this range have been published (Shepherd et al. 2001; Carlberg et al. 2000), whilst an analysis of cosmic star formation history is in preparation (Whitaker et al., in preparation).

2.1 Extension of the CNOC2 survey

In this paper we present follow-up observations of a subset of the CNOC2 sample of galaxies. The goal of the additional observations was to observe wavelength ranges including the Hα and Hβ lines in order to set limits on the reddening of the objects and hence to allow estimation of the unreddened star formation rates for this subsample. As will be shown below, this subsample then allows us to test other means of reddening estimation and hence to obtain reddening measurements for the entire CNOC2 sample.

In order to maximize the run efficiency, masks were designed with slits assigned as a first priority to objects with $0.2 < z_{spec} < 0.37$ (allowing observation of both Balmer lines) and detected [O II] $\lambda 3727$ emission. Second priority was assigned to objects within the
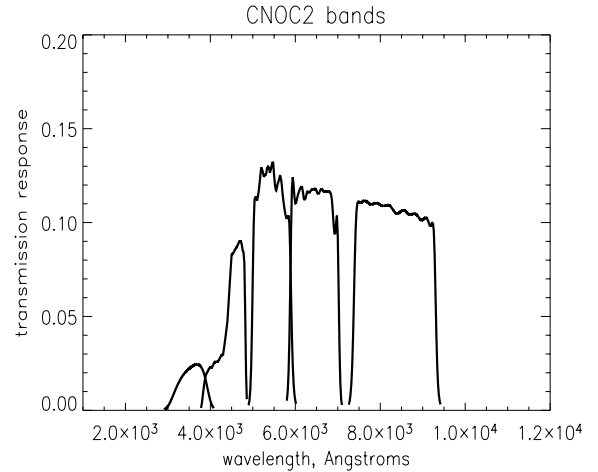
Figure 1. CNOC2 passbands combined with CCD response. From short to long wavelength they are U, B, V, R_C, I_C.

same redshift range, but with no detected [O II], and third priority to galaxies within the CNOC2 magnitude range that did not yet have redshifts. This last sample will not be used in this paper.

Data were taken with the CFHT MOS spectrograph (Crampton et al. 1992) during a four-night observing run in 1999 August. 17 masks containing a total of 719 slits were observed, spread across three of the CNOC2 'patches'. The R300 grism was used, giving a potential wavelength coverage from 4000 to 10 000 Å (depending on slit location), with a dispersion of 5 Å per CCD pixel. A slit width of 1.5 arcsec was used, giving a nominal spectral line full width at half maximum (FWHM) of 3.4 pixel or 17 Å.

The data were reduced in IRAF (Tody 1993).[2] The reduction was based on a slightly modified version of the CNOC2 standard reductions of Yee et al. (2000). The steps included object finding, tracing and extraction, wavelength calibration, flux calibration, and interpolation over bad sky subtraction and zero-order residuals. Error vectors were carried through the same procedure.

2.2 Measurement of the Balmer decrement from CNOC2

Our own purpose-written code (Whitaker et al., in preparation, based on the code by Balogh 1999) was used to measure the fluxes and equivalent widths of the Balmer lines in each spectrum. In brief, the code measures the flux and equivalent width over pre-defined spectral windows, set for each line. Each window includes two continuum regions and a line region. We perform a 1.5σ clip on the continuum regions to reject outliers and improve the quality of the continuum fit. Table 2 shows the windows we use for Hα and Hβ in this study. We note that our Hα definition is similar to that of Balogh et al. (2002), with one minor modification: we use a wider line region in order to fully encompass the Hα+[N II] flux in our measurement; this necessarily reduces the size of the blue continuum region by 1 Å. This should have minimal effect on the quality

---

[1] V photometry is actually g-band data calibrated to the V system based on Landolt standards.

Table 2. Windows used for Hα and Hβ in this study.

Feature	Window (Å)	
	continua	line
Hα	6490–6536; 6594–6640	6537–6593
Hβ	4785–4815; 4911–4931	4821–4901

of the continuum fits. The Hβ window we use is identical to that of Dressler & Shectman (1987).

While it is true that the continuum fit is obtained from only seven (four) independent points for Hα (Hβ), the actual number of data points used in the fit is considerably more: 23 (13) for Hα (Hβ), i.e. ∼3 data points per resolution element. As a result, any spurious points, from cosmic rays or the like, will be safely rejected without substantially reducing the quality of the fit.

Fig. 2 shows three typical spectra from our sample – the window regions are overplotted.

Error estimates on the equivalent widths are computed using the formulae set out by Bohlin et al. (1983). For the error on the flux measurement we employ the following rule:

$$\sigma_F = F \frac{\sigma_W}{W}, \tag{1}$$

where F and W signify the measured flux and equivalent width, and σ_F and σ_W their respective errors.

The original CNOC2 data set contains multiple observations of certain galaxies, and by using these we are able to assess whether we systematically underestimate or overestimate the equivalent-width errors. Our procedure is to compute for each pair of repeats a quantity ϵ such that

$$\epsilon = \frac{W_1 - W_2}{\left(\sigma_1^2 + \sigma_2^2\right)^{1/2}}, \tag{2}$$

where W and σ are as in equation (1), and the subscripts '1' and '2' refer to the separate observations. The perfect case is where the distribution of ϵ is a unit Gaussian of mean zero. This would imply that we have accurately measured the errors and that there are no systematic underestimates or overestimates.

Such a unit Gaussian is not found using the raw errors, and so they are scaled according to the following equation:

$$\sigma_{\text{true}}^2 = A\sigma_{\text{raw}}^2[1 + B(\sigma_{\text{raw}}^2 - ave^2)], \tag{3}$$

where A and B are multiplicative factors to be determined, and ave is the average raw [O II] equivalent-width error larger than 2 Å. We recompute the distribution of ϵ for a range of A and B and check whether it is a unit Gaussian. The process is repeated until a unit Gaussian is found.

The same scaling we apply to the [O II] errors is then applied to the Hα errors in this work (see Whitaker et al., in preparation, or Balogh 1999 for the full details of this procedure).

### 2.3 Correction for [N II] emission and stellar absorption

The window we employ in our spectral measurement code encompasses both the Hα and [N II] lines. We cannot separate the two lines in our data, nor are we able to accurately de-blend them using Gaussian fitting tools (e.g. SPLOT in IRAF) since the data is not of sufficiently high resolution. Instead, to correct for [N II] we assume an [N II]/Hα ratio of 0.5 (as per Kennicutt 1992). This is a simple approximation; however, a by-eye examination of spectra in our sample reveals that it is not obviously incorrect (see e.g. Fig. 2). Using an extreme value for the N II/Hα ratio such as 0.33, which Kennicutt & Kent (1983) find for H II regions, results in a difference of ∼0.4 in A_V compared with the [N II]/Hα = 0.5 case. This value for H II regions does not incorporate the effects of interstellar gas with its higher mean [N II]/Hα ratio, and since our spectra are from the galaxy as a whole rather than from individual H II regions we assume the 0.5 factor to be the most reasonable.

The Balmer emission lines sit on top of stellar absorption as a result of the presence of young and intermediate-age stars in the line-emitting galaxy, so any measurement of their fluxes must take this into account. This is particularly true for Hβ, where one often finds an emission line sitting in an absorption trough (see the middle right-hand panel of Fig. 2 for an example of this).

Again, owing to the restrictions imposed by the data, we are not able to reliably fit the emission and absorption components
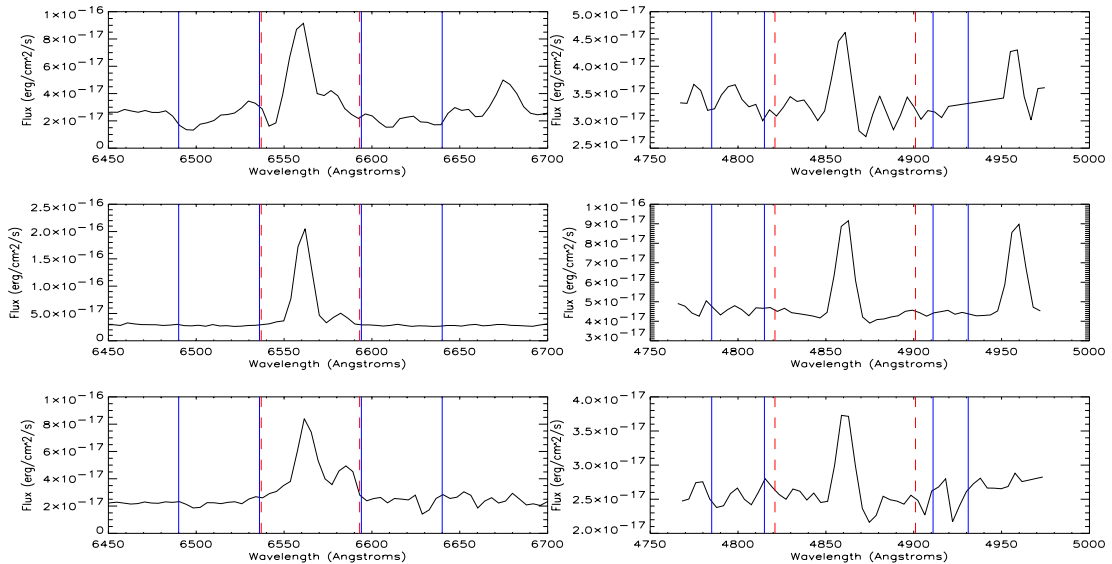
Figure 2. Three typical spectra from which we measure the Balmer decrement. The left column shows the Hα region, the right column shows the Hβ. The window regions are overplotted: the solid (blue) lines show the continua regions, the dashed (red) lines the line region. The spectra are shown in rest-frame wavelength, and the mean redshift of the whole sample is ∼0.286.
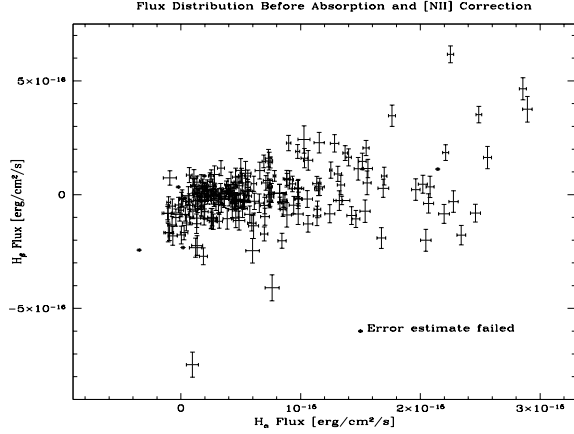
Figure 3. The flux distribution of Hα and Hβ prior to corrections for [N ɪɪ] and stellar absorption.

Figure 4. The flux distribution of Hα and Hβ after corrections for [N ɪɪ] and stellar absorption. Crosses are sources with a detection of at least 3σ in both Hα and Hβ, arrows denote sources with an Hα detection of at least 3σ but where the Hβ flux has been reset to a 3σ limiting value. Sources in which neither line could be measured at above 3σ are not plotted.

separately within each line, so instead choose to apply the corrections used by the Sloan Digital Sky Survey (SDSS: Hopkins et al. 2003). The SDSS team measure a median absorption at Hα of 2.6 Å (note that we do not employ their correction of 1.3 Å since we are using a window measurement method to obtain our fluxes, not the Gaussian fits of the SDSS pipeline). For the Hβ correction, we use the value for Sb Galaxies (2 Å) given by Miller & Owen (2002), also used by the SDSS team.

In addition to making the above two corrections to the flux measurements, we also do the following. For sources with a secure Hα detection but either a low significance Hβ detection in emission, or detection at any significance level of Hβ in absorption, we reset the Hβ flux to be its 3σ error value. For the emission cases this is an obvious step. For the absorption cases, however, it should be stated that the maximum Hβ *emission* flux is still the 3σ value – the absorption may of course be larger than this, but since the galaxies are emitting at Hα, they must also be emitting at Hβ.

Figs 3 and 4 show the flux distribution of Hα and Hβ before and after, respectively, the above corrections for [N ɪɪ] and stellar absorption. In Fig. 4 the reset Hβ values are plotted as arrows, indicating an upper limit on the flux.

2.4 Balmer line detections and limits

We divide the 719 objects observed in the extension to the CNOC2 data set as follows.

(i) 367 objects do not have redshifts in the original CNOC2 survey and so are removed from our sample.

(ii) Of the remaining 352 objects, 46 are removed, either because of skylines that obscure the Hβ line (33 objects), or because of problems with the noise measurements arising from the data reduction procedures (13 objects).

This leaves 306 objects, and of this subset

(i) 46 objects possess both emission lines measurable at above 3σ accuracy (we refer to these as 'measure' cases);

(ii) 153 objects have only Hα measurable to an accuracy above 3σ – Hβ is not measurable to such accuracy in these spectra (we refer to these as 'limit' cases, i.e. we obtain a lower limit to the reddening for these objects);

(iii) 107 objects have neither Hα nor Hβ emission detectable at above 3σ accuracy, and thus we are unable to estimate a lower limit on the reddening from these galaxies.
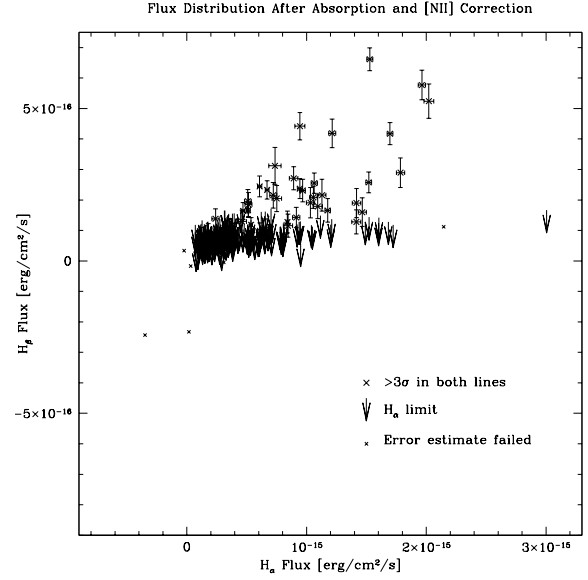
Of the set of 46 measurements, five of them fall $> 3\sigma$ below zero and, of these five, four are removed (see below). This leaves 42 measured sources for the analyses carried out later in this paper. We note that, in a large enough sample, some objects are expected to lie 3σ below zero reddening, owing to the nature of the statistics. We now describe the five objects in question.

(i) Three objects appear to be blends, where two (or more) galaxies are co-extracted from the slit; it is impossible to derive a reddening measurement from these spectra.

(ii) One object has an error in the noise vector.

(iii) One object has a high-quality spectrum but a relatively small [N ɪɪ] flux. Our methodology of using a coarse correction for the [N ɪɪ] flux serves to push extra objects into the 3σ-below-zero-reddening range (in addition to those we naturally expect from Gaussian statistics). This object is retained in the sample.

Of the set of 153 lower-limit cases we note that 70 produce limits below zero reddening. Again, given our error approach, this is not surprising.

The mean redshift of the sample of 'limits' and 'measures' (Fig. 4) is ∼0.262, while that of every object (Fig. 3) is ∼0.286.

2.5 Selection effects

The 'measures' sample we define and use in this work is subject to certain selection effects.

The observations are clearly most sensitive to galaxies that have strong emission lines and low to moderate A_V. Any galaxies with weak emission lines and moderate A_V will be lost from our sample since the lines will have been diminished to the extent where they are undetectable. This is also true for galaxies with large extinction – at least Hβ, if not both Balmer lines, will have been diminished by too great an amount to be detectable. The best that can be accomplished in that case is to estimate a limit on the extinction, as we have done here.

The problem of skyline contamination of the Hβ line is one that all projects attempting reddening measurements in external galaxies will suffer from. However, this will not affect our results unless there exists a strong correlation of extinction with redshift such that certain extinctions occur at certain redshifts where the Hβ line is obscured. Given the narrow redshift range of the survey and the strength of correlation that would be required it is not anticipated that this will be an issue.

2.6 Calculation of extinction from the Balmer ratio

The Hα and Hβ Balmer lines provide a probe of extinction for the optical region of the spectrum – their un-extincted intensity ratio is well known from atomic physics (Osterbrock 1989) and is 2.86 in typical nebula conditions ($T = 10\,000$ K, $n_e = 10^2 - 10^4$ cm^{-3}). Their ratio thus leads to the Balmer optical depth, τ, and can therefore provide a measure of the dust content by way of the internal reddening along the line of sight (e.g Calzetti, Kinney & Storchi-Bergmann 1994), down to an optical depth of $\tau \sim 1$.

The observed ratio, R_{obs}, of Hα/Hβ can be related to the reddening to the gas, $E(B - V)_g$, according to the following equation (e.g. Calzetti, Kinney & Storchi-Bergmann 1996):

$$E(B - V)_g = \frac{2.5[\log(R_{obs}) - \log(R_{int})]}{k(H\beta) - k(H\alpha)}, \qquad (4)$$

where R_{int} is the intrinsic Hα/Hβ ratio of 2.86 and $k(H\alpha)$ and $k(H\beta)$ are the extinction coefficients at the wavelengths of Hα and Hβ respectively (from Calzetti et al. 1993).

The Calzetti curve (Calzetti et al. 1993) was used to compute A_V values from the Balmer decrement, with the lowest measured A_V being -2.25 (this is the source previously mentioned that has low [N II] flux) and the highest being 5.15. These values are typically accurate to 30 per cent; the mean of the ratio $A_V/\sigma(A_V)$ is 0.27. Fig. 5 shows histograms of the 42 Balmer[A_V] values as well as the 153 'limit' cases.

The choice of extinction curve is one of the sources of uncertainty – the extinction curves of local galaxies do differ (see, for example, the review by Calzetti 2001a). The largest differences are due to the strength of the feature at $\sim$2175 Å, thought to result from graphite grains, amorphous carbon or polycyclic aromatic hydrocarbon (PAH). However, for the Balmer lines, this feature is not a factor: the Balmer lines are sampling the longer-wavelength region where the extinction curves have a more constant slope, so that differences are reduced. The main difference between the curves here can be parametrized by the chosen value of the ratio R_V, which is the total-to-selective extinction ratio in the V band (Calzetti et al. 1993). In these investigations $R_V = 4.05$ is used.

3 BALMER EXTINCTION VERSUS PHOTOMETRY

Are we able to compare photometry-derived extinction values, hereafter Phot[A_V], with Balmer[A_V] values in order to better understand the accuracy and/or reliability of photometry-derived extinction measurements?

The crucial point here is that the Balmer decrement probes the extinction A_V of the ionized gas in the source – the extinction of molecular clouds/H II regions (star-forming regions), $E(B - V)_g$. In the SED template-fitting method in which photometry in a number of bands is compared with a library of templates with variable internal A_V, the resulting best fit returns a template type, redshift and A_V. In this case the extinction results from the ISM, which acts on the stellar continua within the galaxy as a whole. Thus Phot[A_V] probes the dust obscuration of the stellar continuum, $E(B - V)_s$. This is more complicated than just the total amount of dust between the observer and the source, as would be the case for a single star, as folded into this is information on scattering and the geometrical distribution of dust within the galaxy.

Since the Balmer and photometry methods are probing different regimes of the galaxy extinction, they might well be expected to
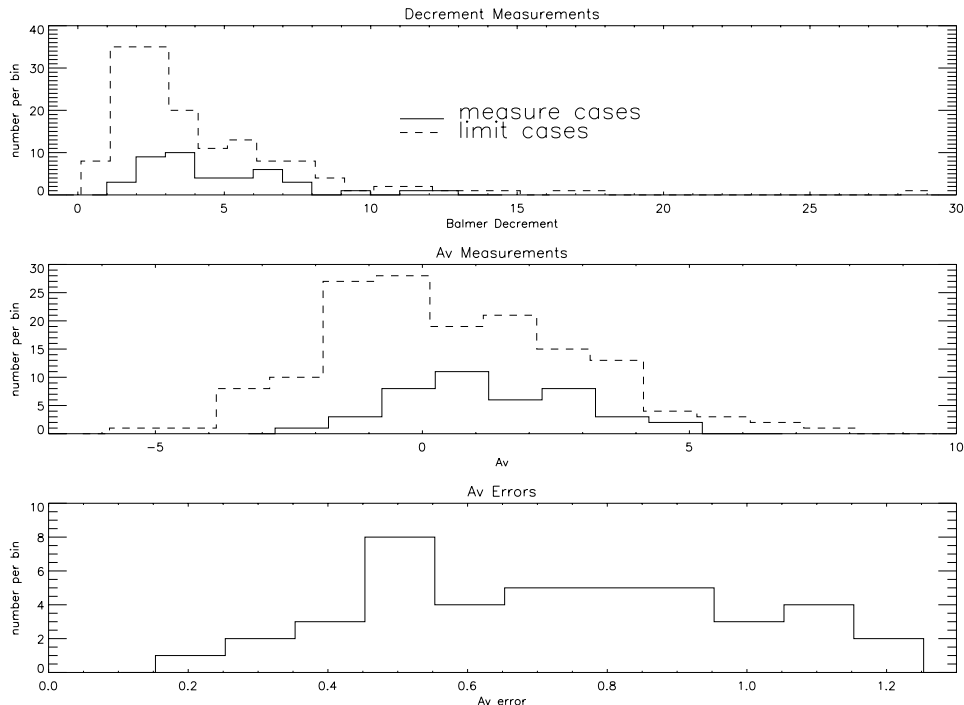
Figure 5. The distribution of Balmer decrements (top), Balmer[A_V] values (middle) and associated errors (bottom). The solid line shows results for the sources measured at above 3σ accuracy, the dashed line the 'limit' cases (in this case the decrements and Balmer[A_V] values are lower limits).

give differing results. In a galaxy such as a starburst, where there is a significant amount of heavily obscured star formation, the two regimes will be linked – the galaxy's overall emission is dominated by the young star formation. At the opposite end of the scale, an elliptical galaxy will have little dust or ongoing SFR. In this case the two measures are uncorrelated (although both measures are likely to be low). For intermediate-type galaxies the relationship falls somewhere between these two regimes.

The following relationship between the colour excess of the stellar continuum and of the nebular emission lines is given in Calzetti (2001b) and Calzetti (1997):

$$E(B - V)_s = (0.44 \pm 0.03)E(B - V)_g. \tag{5}$$

This follows on from Calzetti et al. (1994), in which 39 starburst and blue compact galaxies were used to derive an *effective* extinction law. From this, it was found that the difference between the optical depth to the Balmer lines, and to the underlying stellar continuum at the lines was approximately a factor of 2. Calzetti's relationship is a purely empirical one but it has often, in the past, been assumed to yield the most appropriate reddening corrections for the integrated light of extended star-forming regions or galaxies (e.g. Calzetti et al. 2000; Westera et al. 2004). Here we start with this ratio of 0.44 but then consider other possible values in order to see how the results are affected.

4 PHOTOMETRIC METHODOLOGY

The main outcome of applying a redshift code is the best-fitting redshift, extinction and template SED of each source. In the template-fitting procedure, the observed galaxy magnitudes are converted for each ith photometric band into an apparent flux, f_i^{obs}. The observed fluxes can then be compared with a library of template (T) fluxes, f_i^{templ} (z, T, A_V), as calculated by convolving the template SEDs with the filter response functions. The reduced χ^2, χ^2_{red}, is computed for each point in the hypercube of redshift/template/A_V flux values and the best-fitting solution is selected.

4.1 The templates

Here we use six galaxy templates, as presented in B04: E, Sab, Sbc, Scd, Sdm and starburst galaxies. These were generated via spectrophotometric synthesis (see Berta et al. 2004 for more on this procedure) of several simple stellar populations (SSPs), each weighted by a different SFR and extinguished by a different amount of dust, and were designed to reproduce in more detail the empirical low-resolution templates of RR03. These SSPs have been computed with a Salpeter initial mass function (IMF) of between 0.15 and 120 solar masses, adopting the Pickles (1998) spectral atlas and extending the atmospheres outside the original range of wavelengths with Kurucz (1993) models from 1000 to 50 000 Å, as described in Bressan, Granato & Silva (1998). Nebular emission is added by means of case B H II region models computed through the ionization code CLOUDY of Ferland et al. (1998). The adopted metallicity is solar. In addition to the galaxy templates, two AGN templates can be considered. However, for the CNOC2 sample used here it was found that the AGN templates did not provide the best fit to any of the sources (as expected based on their spectra), so in this paper only the six galaxy templates are considered. They are plotted in Fig. 6.

One important consideration for the investigations here, and template-fitting codes in general, is that the extinction output by the photometric redshift codes refers to the Phot[A_V] values of the
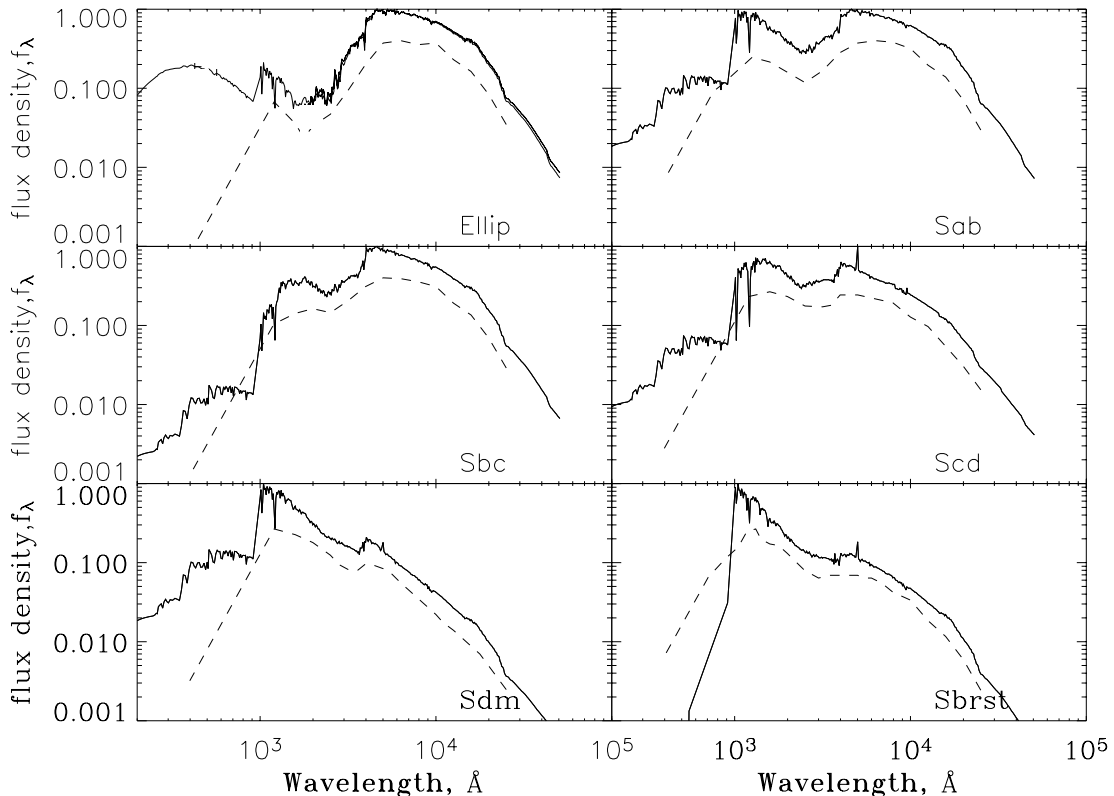
Figure 6. The six galaxy templates used. Dashed lines show the original RR03 templates (offset for clarity), solid lines show the SSP-generated versions, along with extension into the far-UV (sub-1000 Å) as discussed in B04.

Table 3. Final parameters for the two photometric redshift codes.

	ImpZ	hyperz
Templates	E, Sab, Sbc, Scd, Sdm, Sb	Sab, Sbc, Scd, Sdm, Sb
M_B limits	$[-22.5 - 2\log_{10}(1 + z)] < M_B < -13.5$	not constrained (but set by $z_{\rm spec}$)
A_V limts, A_V step	$-0.3 \leqslant A_V \leqslant 3.0$, step 0.1	$0.0 \leqslant A_V \leqslant 3.0$, step 0.27
Reddening law	Cardelli 1989	Calzetti 2000
Galactic extinction correction?	Yes	No
Constrained to $z_{\rm spec}$?	One run unconstrained, one run constrained	Yes
Cosmology	$\Omega_0 = 1$, $\Omega_\Lambda = 0.70$, $H_0 = 72\,{\rm km\,s^{-1}\,Mpc^{-1}}$	$\Omega_0 = 1$, $\Omega_\Lambda = 0.70$, $H_0 = 72\,{\rm km\,s^{-1}\,Mpc^{-1}}$

best-fitting solutions. However, these values are those of the variable A_V, which has been *added* to the template in question. In addition to this there is also the issue of the *inherent* A_V of the templates. This is problematic in that the templates originate from empirical templates drawn from observations, along with alterations found to optimize redshift solutions in previous studies. Their regeneration via spectrophotometric synthesis, where the overall template is reproduced using a small number of simple stellar populations (SSPs), is designed to give some insight into the underlying physics of each template. Hence an overall A_V can be defined, based on the A_V values of the contributing SSPs.

In B04 these inherent A_V values (ranging from 0 for the elliptical to 0.74 for the starburst) were given. It is, however, possible to reproduce the same[3] overall template using different proportions of SSPs with differing A_V contributions. For example, the starburst template can be generated from young SSPs to give the 'same' overall template, but with a total A_V of either 0.05 or 0.74. Similarly, the Scd can be generated with an A_V of 1.6 or 0.27. Clearly, then, we should not take the inherent A_V values of the SSP solutions at face value (we note that in the case of fitting SSPs to spectroscopic data most of these degeneracies can be expected to be broken). Empirically, we would expect the inherent A_V of the late-type galaxies (Sab, Sbc, Scd, Sdm) to have an extinction to the gas of perhaps $A_V \sim 0.5$–1.0, and starbursts to be more dusty ($A_V > 1.0$, say).

These SSP degeneracies imply, then, that photometric data are not able to constrain the extinction to an accuracy of less than perhaps ± 1 in A_V. If this is the case, one would not expect a correlation to be found between the Phot[A_V] solutions and the Balmer[A_V], even if the two methods were probing the extinction to the same regions of the galaxy. The results in Section 5 will show that this is overly pessimistic, thus implying that SSP fitting considers more possible combinations than actually occur – there are additional constraints imposed in reality due to the nature of star formation, fuelling and feedback that such fits do not incorporate. Since the details of inherent A_V are undetermined, inclusion in the analysis would introduce an additional free parameter. For this relatively small sample there are insufficient data to constrain this properly, so here it is merely noted that inherent A_V is an additional complication and that it is expected to act to increase the Phot[A_V] estimates. If the issue of inherent A_V is a large one then we would expect it to swamp any Phot[A_V]/Balmer[A_V] correlation – Section 5 will show that, in practice, this is not the case.

4.2 The ImpZ code

This code was presented in B04. Massarotti, Iovino & Buzzoni (2001) have shown that, at high redshift, correct treatment of internal (to the galaxy) dust reddening (the interstellar medium) and

IGM attenuation (between the galaxy and observer) are the main factors in photometric redshift success. The effect of internal dust reddening for each galaxy is alterable via fitting for A_V, using the reddening curve of Savage & Mathis (1979), and the effects of the IGM are incorporated as in Madau et al. (1996). Observed fluxes are compared with template fluxes for $0.01 \leqslant \log_{10}(1 + z) \leqslant 0.90$, equivalent to $0.02 < z \leqslant 6.94$.

Galactic extinction in the CNOC2 regions is low; using the extinction–wavelength relation in Cardelli et al. (1989) we can calculate Galactic extinction in each of the CNOC2 bandpasses and correct for it (see Table 1), although the resulting corrections are negligible.

For the CNOC2 sample survey the following parameters were used, adapted from investigations presented in B04.

Templates: the six galaxy templates (E, Sab, Sbc, Scd, Sdm and Starburst), with IGM treatment and Galactic extinction corrections.

Internal extinction: A_V limits of -0.3 to 3.0 in the A_V freedom. Negative A_V was allowed since the inherent A_V of the templates is non-zero. For the elliptical template, A_V can take the value zero only, since ellipticals are not expected to have significant internal extinction.

Magnitude limits: B04 found it necessary to apply redshift-dependent absolute magnitude limits to exclude unphysical solutions (such as superluminous sources at high redshift). Here, the same limits are used: absolute magnitude limits of $[-22.5 - 2\log_{10}(1 + z)] < M_B < -13.5$ for galaxies.

Prior: ImpZ usually applies a prior expectation that the probability of a given value of A_V declines as $|A_V|$ moves away from 0. This is introduced by minimizing $\chi^2_{\rm red} + \alpha A_V^2$ ($\alpha = 2$ here) rather than χ^2. This use of a prior can be viewed as a weak implementation of Bayesian methods and was reached based on degeneracy studies in B04 and RR03. For this investigation it was of interest to turn off this prior. This is because the Balmer[A_V] values of the sample range from -2.25 to 5.15, or for the starlight (multiplying by 0.44) from -1 to 2.3. Hence applying an A_V prior would naturally tend to limit the A_V solutions to values in a similar range, regardless of the input A_V limits, and so some correlation could be achieved simply because all the data in the sample have Balmer[A_V] values that equate to the lower end of the A_V parameter space.

Table 3 shows the final parameters used in ImpZ and hyperz.

4.3 hyperz

hyperz is described in full in Bolzonella et al. (2000). Here we present an overview of the code and the parameters we used for each run. The hyperz code also uses SED fitting in its determination of photometric redshifts, and for this work we chose to use the same templates as in ImpZ. However, for the investigations presented here, we choose to apply hyperz for a 'best-case' scenario in which both the redshift and template type are constrained in order to optimize

---

[3] Here, 'same' means from the point of view of flux through a set of broad-band filters.

Table 4. Statistical results for the various comparisons between Balmer[A_V] and Phot[A_V].

	$\overline{\Delta A_V}$	σ_{A_V}	outlier fraction, η
IMPZ, $\gamma = 0.44$	−0.2	0.83	50 per cent
HYPERZ, $\gamma = 0.44$	−0.3	0.84	50 per cent
IMPZ, $\gamma = 0.25$	−0.4	0.72	38 per cent
HYPERZ, $\gamma = 0.25$	−0.5	0.76	57 per cent
IMPZ/HYPERZ comparison	−0.09	0.53	17 per cent

the resulting accuracy of the extinction values. In order to create such a 'best-case' scenario, we choose to remove one degree of freedom by constraining the photometric redshift solution to within $z_{spec}/100$ of the known spectroscopic redshift. Furthermore, we choose not to use the elliptical template in the analysis presented, since none of the galaxies with detected Balmer lines are ellipticals based on visual inspection of the spectra.

We do not correct for Galactic extinction when running HYPERZ. This correction is negligible in comparison with the photometric errors (see Table 1 for extinction across the CNOC2 patches) and would not affect the results. Any non-detections in a given band were replaced with a flux of zero, the error being the limiting flux in the band (see Table 1 for 5σ limits). Ideally, one would want to provide the measured flux in an aperture placed at the location of the object even when that measurement is fainter than the nominal flux limit of the survey and the resulting value has a very poor signal-to-noise ratio. However, the CNOC2 catalogue used here has had such measurements replaced by a 'non-detection' flag. Thus the best treatment in the template-fitting procedure is to restrict solutions to those that predict the flux in the non-detected band to be at or below the flux limit in that band.

The HYPERZ code was run in its standard form, with the flat, $\Omega_\Lambda = 0.70$ cosmological model with $H_0 = 72\,\mathrm{km\,s^{-1}\,Mpc^{-1}}$ used elsewhere in this paper, and variable A_V in the range $0 < A_V < 3$. Table 3 shows the parameters used in the final setup for IMPZ and HYPERZ.
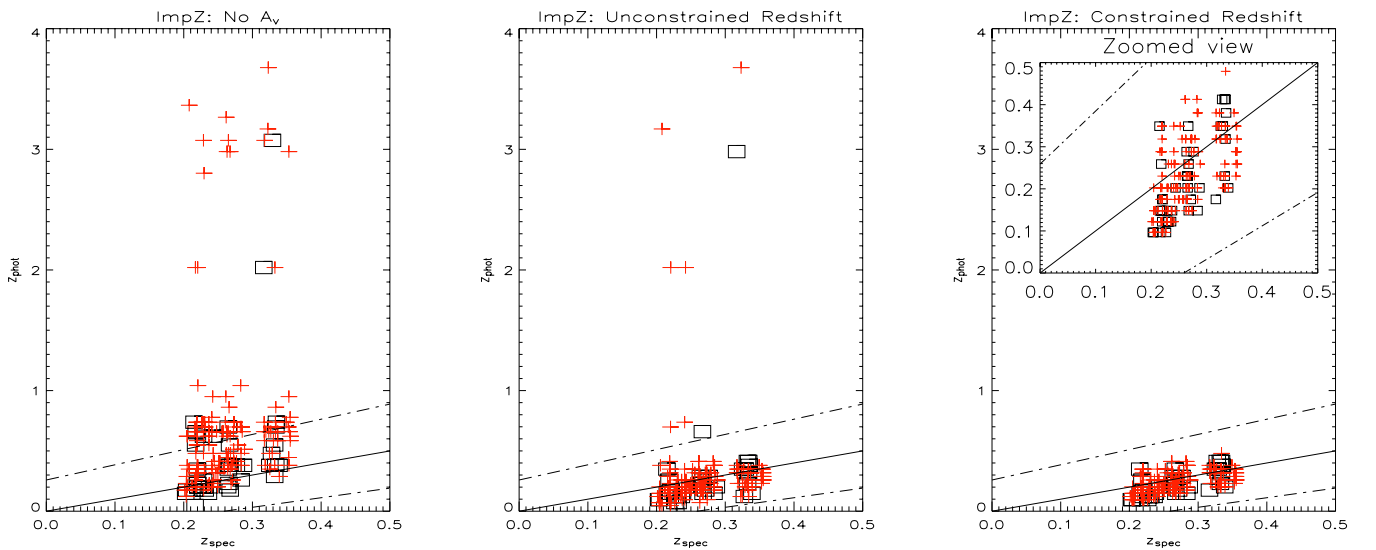
5 RESULTS

5.1 IMPZ redshifts

First, it is of interest to see how successful the photometric redshifts are when there is no A_V freedom – that is, $A_V = 0$ in the solutions. The results of this are plotted in the left-hand panel of Fig. 7, for 'measure' cases (black squares) and 'limit' cases (red crosses). It is immediately clear that not allowing A_V freedom has caused many of the IMPZ solutions to be incorrect: the code has been forced to substitute (incorrectly) additional redshift in place of the reddening action of dust. Indeed, 11 of the 42 'measure' and 70 of the 153 'limit' sources (48 per cent of the sample) have photometric redshifts that lie outside the $\log(1 + z_{spec}) \pm 0.1$ boundaries.

If we now run IMPZ in the optimal manner, as discussed in Section 4.2, so that now A_V freedom is allowed, the solutions improve dramatically. IMPZ was highly successful at deriving photometric redshifts in close agreement with the spectroscopic values for 40 of the 42 'measure' and 147 of the 153 'limit' sources (95 per cent of the sample). Note that we consider redshift solutions in the range [0:7]. There were eight (two 'measure' and six 'limit') sources that obtained solutions at incorrect redshifts as a result of degeneracies in [z, template, A_V] space. We measure the accuracy of the photometric redshifts via the rms scatter σ_z, calculated as follows:

$$\sigma_z^2 = \sum \left(\frac{z_{phot} - z_{spec}}{1 + z_{spec}} \right)^2 / N, \tag{6}$$

with N being the number of sources with both spectroscopic redshifts and photometric redshifts. For these data, the rms scatter $\sigma_z = 0.32$ when including the eight outliers, or 0.07 when they are excluded. The comparison of spectroscopic and IMPZ redshifts is plotted in the middle panel of Fig. 7.

IMPZ is therefore successful at returning accurate redshifts. However, can it also provide a measure of the extinction compatible with that implied by the Balmer decrement? Since two of the 42 'measure' sources obtain an incorrect photometric redshift this means that their extinction values are also likely to be incorrect. In order to remove this (small) source of error in the following comparisons

Figure 7. Photometric redshifts from IMPZ. Comparison of spectroscopic and IMPZ-derived redshifts for 'measure' cases (black squares) and 'limit' cases (red crosses). The left-hand panel shows results when A_V freedom is not considered; the middle panel shows results for unconstrained redshift and A_V space; and the right-hand panel shows results for redshift space constrained to be within 0.05 in $\log(1 + z_{phot})$ of z_{spec}, but A_V unconstrained. Dot-dashed lines denote an accuracy of 0.1 in $\log(1 + z)$, a typical photometric redshift accuracy.
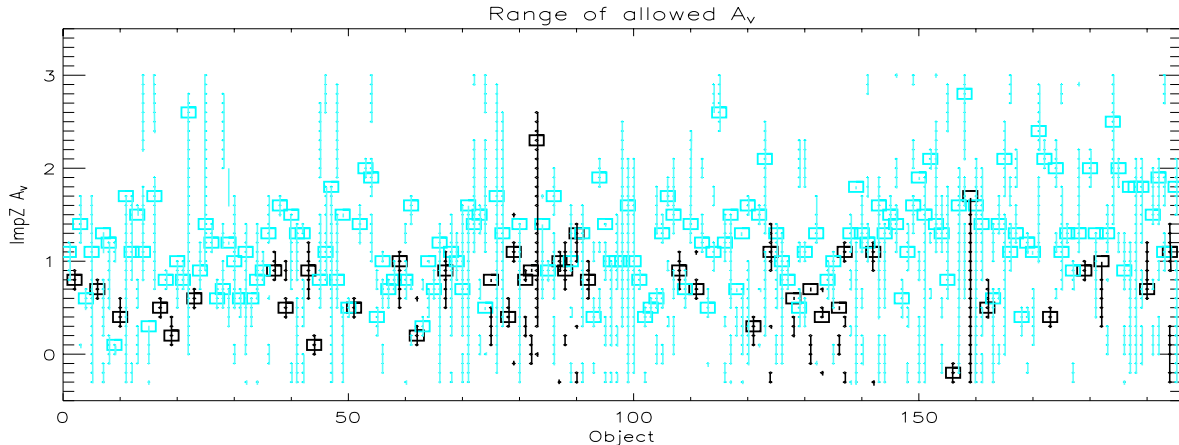
Figure 8. IMPZ A_V allowed values. The range of A_V parameter space for each source that provides a solution with a reduced χ^2 within $\chi^2_{min}+1$ and that is at or near the correct redshift (within 0.05 of $\log[1+z_{spec}]$). 'Measure' sources are shown as black lines, 'limit' sources as cyan lines. The best A_V solution value is indicated as a black ('measure' case) or cyan ('limit' case) square.

with the Balmer-derived extinction, we now constrain the redshift range explored by IMPZ to lie within 0.05 in $\log(1+z_{phot})$ of z_{spec} (plotted in the right-hand panel of Fig. 7). Now, good solutions are found for all 42 'measure' cases and 153 'limit' cases, with $\sigma_z = 0.06$. It is the resulting IMPZ A_V values from this setup that are considered from now on in the investigation.

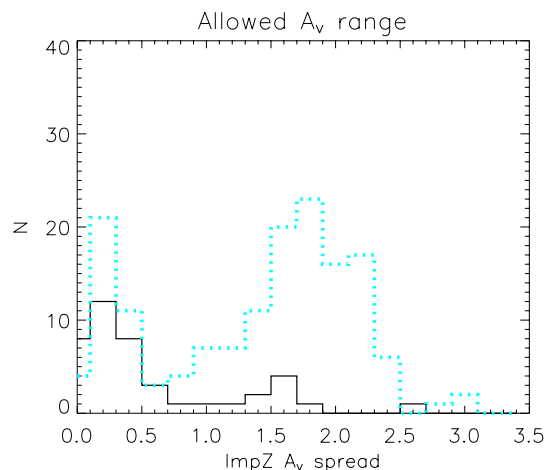## 5.2 Range of IMPZ A_V allowed values

Although we wish to explore the accuracy of the extinction output from redshift codes by comparing to a sample with Balmer-derived measurements, we can also obtain an internal estimate of how well constrained the [z, template, A_V]-solution is from the reduced χ^2 distribution. For the solution with the minimum χ^2, χ^2_{min}, the following question can be asked: what range of A_V produces a fit at or near the correct redshift (within 0.05 of $\log[1+z_{spec}]$), with a reduced χ^2 within $\chi^2_{min}+1$?

The results of asking this question of each source are illustrated in Fig. 8. It can be seen that, for the majority of 'measure' cases (black), the A_V is quite well constrained, in most cases to within 0.3 or so in A_V. Note that the lines in this plot can be discontinuous; for example, object 150 in the plot has a best-fitting A_V of 1.9 but has reasonable solutions in the A_V ranges −0.3 to 0.4 and 0.8 to 1.1 which arise from fitting two other templates to the source. It is of interest to note that, whereas 57 per cent of 'measure' cases do not have discontinuous solutions, this is only true for 43 per cent of the 'limit' (cyan) cases. Thus, determining the A_V via photometry for these sources is more problematic, just as it is via the Balmer ratio method. Considering the 'measure' cases in more detail, there are two objects for which the A_V is poorly constrained (objects 83 and 159 in the figure, evidenced by their long black lines). Their best-fitting A_V values are, respectively, 2.3 and 1.7, making them the most heavily extincted of the IMPZ 'measure' cases. Comparison with their Balmer[A_V] (3 ± 1 and −1.6 ± 0.5 respectively) would support the result for the first source but the Balmer decrement for the second source would imply negative, or zero extinction, arguing against the IMPZ best-fitting result, or resulting in the interpretation that this source is problematic.

Fig. 9 illustrates the width of A_V parameter space that lies within +1 of χ^2_{min} by plotting the distribution of this 'width' value (here the 'width' is simply defined as the maximum allowed A_V minus

the minimum allowed A_V). For 'measure' cases (black) the distribution drops quite steeply with width such that more than half of the sources have a width of 0.4 or less. There is then a slight tail made up primarily of sources that had discontinuous solutions (such as one template with low A_V and another template with higher A_V), whilst the two sources with poorly constrained A_V can be seen as a spike towards the maximum width of 3.3 (i.e the full −0.3 to 3 A_V range). The distribution for the 'limit' cases is more clearly bimodal, with a similar set of reasonably well-constrained sources with an A_V-width of 0.4 or less, but a much larger set of sources with poorly constrained A_V. Again, this is likely to be a result of the nature of these 'limit' sources for which the dust extinction is hard to determine (via either the Balmer lines or photometry).

This analysis suggests that the photometric redshift solution has an inherently low extinction precision (at least with five-band photometry), such that A_V is precise to perhaps only 0.3 for most sources, and is poorly constrained for a small subset. Rather than defining this internally estimated width value as the error in the Phot[A_V] value, we choose instead to take the opposite approach for the comparison with the Balmer[A_V]. We will take the Phot[A_V]

Figure 9. Histogram of the width of IMPZ A_V allowed values. Distribution of the width of A_V parameter space (defined by the minimum and maximum allowed A_V) that lies within +1 of χ^2_{min}. 'Measure' sources are shown as a black line, 'limit' sources as a cyan dotted line.
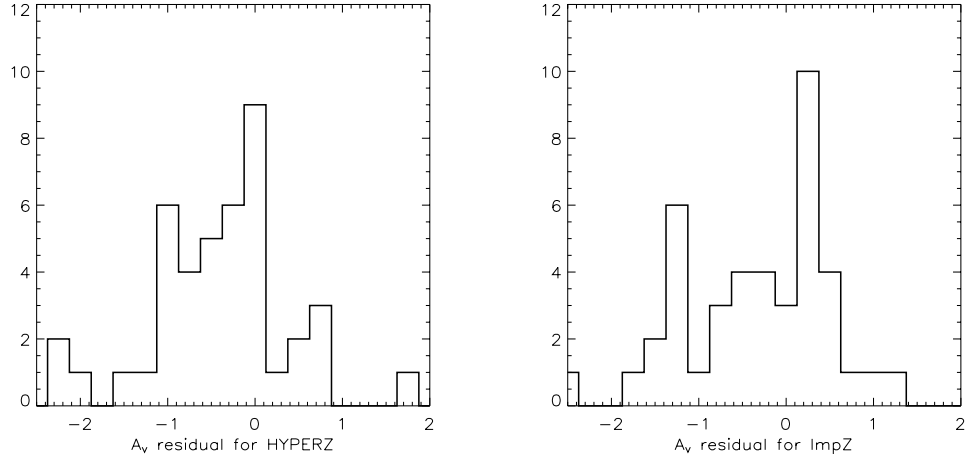
Figure 10. A_V residuals for HYPERZ (left) and IMPZ (right). The residual is $0.44 \times \text{Balmer}[A_V] - \text{Phot}[A_V]$.
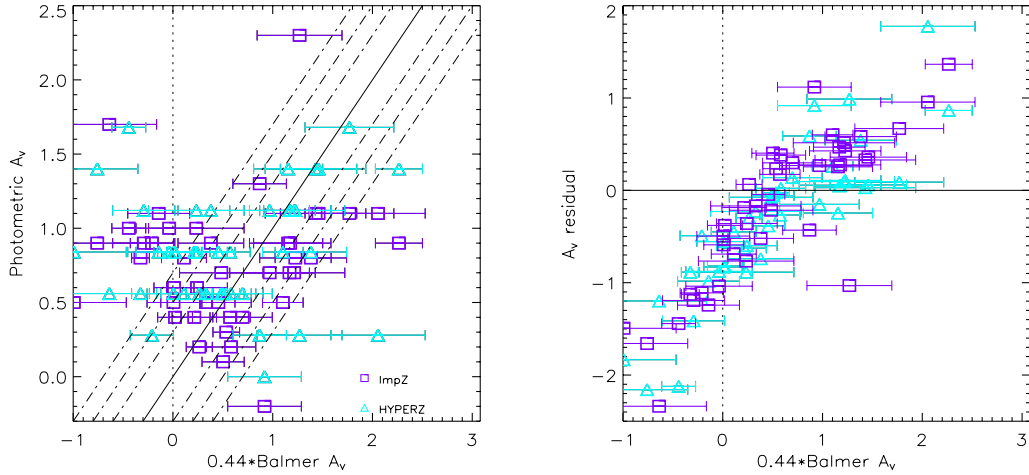
Figure 11. Left: A_V results for HYPERZ (cyan triangles) and IMPZ (purple squares). The plot is of the Balmer[A_V] (multiplied by the Calzetti (2001) factor of 0.44) versus the Phot[A_V]. Dot-dashed lines denote residuals of 0.3, 0.5 and 0.7 in A_V. Errors are not defined for the Phot[A_V] values. Right: A_V residuals for HYPERZ (cyan triangles) and IMPZ (purple squares). The plot is of Balmer[A_V] (multiplied by the Calzetti 2001 factor of 0.44) versus the residual $0.44 \times \text{Balmer}[A_V] - \text{Phot}[A_V]$.

at face value and use the supposed relation with the Balmer[A_V] to provide an external estimate of the precision of the Phot[A_V] measurements.

5.3 IMPZ – comparison with Balmer

We can test how well the Calzetti ratio holds by comparing the Phot[A_V] with $0.44 \times \text{Balmer}[A_V]$. The distribution of A_V residuals for IMPZ is plotted in Fig. 10. It can be seen that there is quite a spread to the distribution, although it is broadly centred on zero. Based on the findings in Section 5.2 on the precision of the Phot[A_V] solutions, some of this spread can be expected to arise from this low precision. Some of it can also be attributed to the accuracy of the Balmer[A_V], which is typically accurate to around 30 per cent.

Fig. 11 plots (purple squares) the IMPZ A_V values and residuals as a function of Balmer[A_V] (multiplied by the Calzetti 2001b factor of 0.44). Note that the IMPZ A_V values have been taken at face-value and have not had an error assigned to them, since we wish to derive an error based on the comparison with the Balmer[A_V] values.

It can be seen that the residuals are smallest for Phot[A_V] values of around 0.5 to 1, and that the residuals increase as we move away

from this region (to either higher A_V or lower/negative A_V). Hence, the correlation to Balmer[A_V] appears to be best for sources of intermediate extinction. It is also clear that none of the sources that were calculated as having negative A_V based on their Balmer lines obtain similar Phot[A_V] values, lending weight to the supposition that the Balmer method has fallen down for these sources as a result of limitations in the technique. The source with the largest Balmer [A_V], of 5.15 ± 0.5, is also the source with the largest residual (of sources with non-negative A_V). Being so extincted, it is likely that this object is quite extreme, so disagreement between the star- and gas-derived extinction measures is to be expected.

Calculating the following statistics:

$$\overline{\Delta A_V} = \sum \left(\text{Balmer}[A_V] - \text{Phot}[A_V] \right) / N, \tag{7}$$

and

$$\sigma_{A_V}^2 = \sum \left(\text{Balmer}[A_V] - \text{Phot}[A_V] \right)^2 / N, \tag{8}$$

and with outliers defined by

$$|\Delta A_V| > 0.5, \tag{9}$$

gives $\overline{\Delta A_V} = -0.2$, $\sigma_{A_V} = 0.83$ and an outlier fraction, η, of 50 per cent. These results are better than one would infer from the

large extinction degeneracies seen in the SSP fitting that were discussed in Section 4.1. Thus, a relationship between Balmer-derived and photometry-derived extinction measures is obtainable, although not a strong one.

5.4 HYPERZ – comparison with Balmer

Applying HYPERZ in a 'best-case' configuration (constraining the HYPERZ redshift solutions to the spectroscopic values and excluding the elliptical template) gives similar statistics of $\overline{\Delta A_V} = -0.3$, $\sigma_{A_V} = 0.84$ and an outlier fraction, η, of 50 per cent. The distribution of A_V residuals for HYPERZ is plotted in Fig. 10. As with IMPZ, the distribution is broad but reasonably well centred on zero.

Fig. 11 plots (cyan triangles) the HYPERZ A_V values and residuals as a function of Balmer[A_V] (multiplied by the Calzetti 2001b factor of 0.44). The residuals are again correlated with the Balmer[A_V], being smallest for Phot[A_V] values of around 0.5 to 1, and the negative Balmer[A_V] sources are again in poor agreement.

Thus, HYPERZ and IMPZ portray a similar correlation to the Balmer[A_V], although the agreement is noisy.

5.5 Comparison of IMPZ and HYPERZ

As well as comparing the extinction outputs of the two photometric redshift codes with the Balmer-derived values, it is instructive to compare them with one another to see if they tend to agree on a similar extinction value for a given source. A plot of IMPZ-A_V versus HYPERZ-A_V is given in Fig. 12.

This shows that the two codes are in reasonable agreement about the extinction of a given source. 25 of the 42 sources (60 per cent) agree within <0.4 in A_V, and 35 sources (83 per cent) agree within <0.5. The main difference appears to be for five sources for which IMPZ gives a high value of $A_V > 0.8$ whilst HYPERZ tends to return a smaller A_V estimate. Two of these sources (this includes object 159 mentioned in Section 5.2) have Balmer decrements that imply negative, or zero, extinction, favouring the HYPERZ result or the interpretation that the sources are problematic. Two others have intermediate Balmer[A_V], consistent with the results of either code, and one has a larger Balmer[A_V] (this is object 83 mentioned in Section 5.2) thus favouring the IMPZ result.

Calculating similar statistics to when comparing with Balmer[A_V], comparison between the A_V values of the two codes
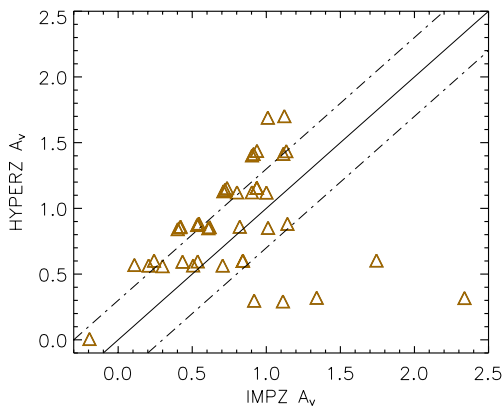
Figure 12. Comparison between IMPZ and HYPERZ: A_V results for IMPZ versus those from HYPERZ. The solid line is exact agreement, and dot-dashed lines are residuals of 0.3 in A_V. Note that for plotting purposes the values have been randomly altered by up to 0.02 in the x and y directions in order to separate points with the same/very similar values.
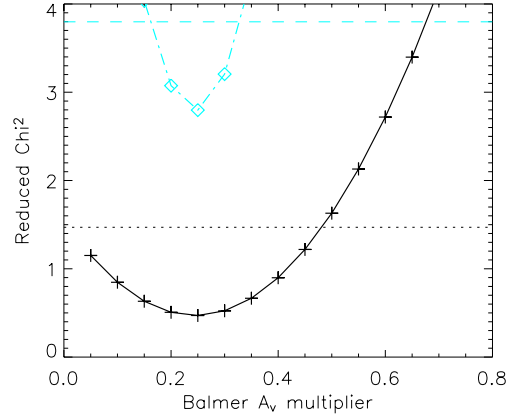
Figure 13. χ^2 analysis. The reduced χ^2 for IMPZ (solid line with crosses) and HYPERZ (dot-dashed line, diamonds) as a function of γ, the chosen ratio between photometrically derived and Balmer-ratio-derived extinction measures. The χ^2 values that are 1 above the minimum in the two distributions are indicated by horizontal lines (IMPZ, dotted; HYPERZ, dashed).

gives $\overline{\Delta A_V} = -0.09$, $\sigma_{A_V} = 0.53$ and an outlier fraction, η, of 17 per cent. This internal consistency check between the two codes gives increased confidence in the photometric redshift template-fitting method as a technique to obtain extinction.

5.6 The Calzetti ratio

We now consider the empirical ratio of 0.44 introduced by Calzetti (1997) and set out in equation (5). We consider a range of other ratios, γ, so that

$$E(B - V)_s = \gamma E(B - V)_g. \qquad (10)$$

Varying this ratio in the range $0.05 < \gamma < 1$, a χ^2 minimization analysis is carried out in order to find the ratio that gives the best correlation between the Phot[A_V] and the Balmer[A_V], weighted by the errors in the Balmer[A_V] measurements. The results of this analysis are shown in Fig. 13. For both IMPZ and HYPERZ, the lowest reduced χ^2 is reached for $\gamma \sim 0.25$. Based on the change in γ that increases the reduced χ^2 by one, the 1σ error on this value is $\gamma = 0.25 \pm 0.25$ for IMPZ and $\gamma = 0.25 \pm 0.1$ for HYPERZ.

The resulting statistical measures, σ_{A_V}, and the outlier fraction, η, are also plotted as a function of γ for the IMPZ and HYPERZ results (Fig. 14). The left-hand panel shows how the rms in the residual, σ_{A_V}, varies with γ. A clear minimum is seen at $\gamma \sim 0.15$ to 0.35 for IMPZ results, and at around 0.2 to 0.4 for HYPERZ. A similar minimum is seen in the range $\gamma \sim 0.2$ to 0.35 for IMPZ results when the outlier fraction, η, is plotted against γ in the right-hand panel. For HYPERZ, the minimum is at around $\gamma \sim 0.3$ to 0.45.

This analysis suggests that, for this sample, the Calzetti ratio of 0.44 is a reasonable choice for γ within the accuracy of the method, although a value of ~ 0.25 is preferred. A choice of $\gamma = 0.25$ gives the following statistics.

For IMPZ: $\overline{\Delta A_V} = -0.4$, $\sigma_{A_V} = 0.72$ and an outlier fraction, η, of 38 per cent.

For HYPERZ: $\overline{\Delta A_V} = -0.5$, $\sigma_{A_V} = 0.76$ and an outlier fraction, η, of 57 per cent.

As before, the distribution of A_V residuals is plotted (Fig. 15). It can be seen that the distribution is more peaked, although offset from zero.
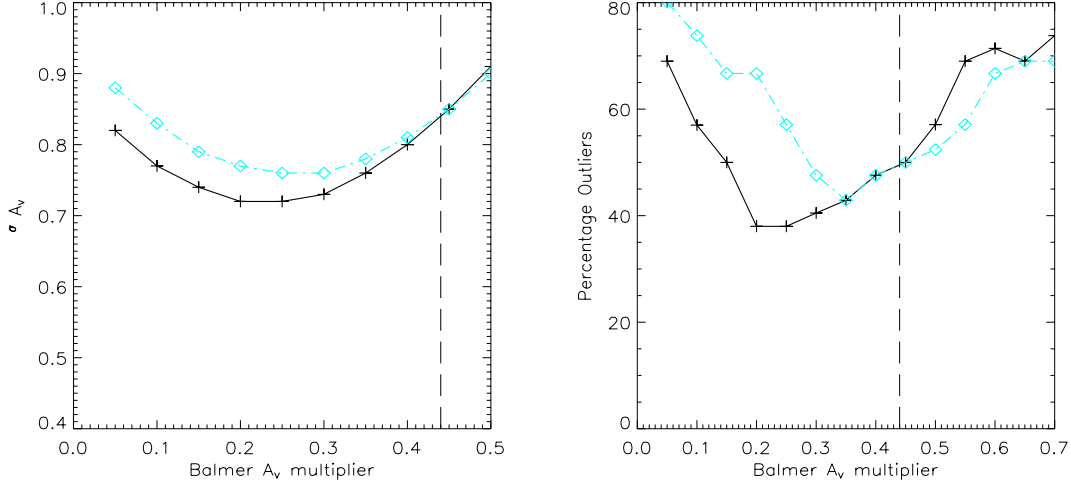
Figure 14. Left: σ_{A_V} for IMPZ (solid line with crosses) and HYPERZ (dot-dashed blue line, diamonds) as a function of γ, the chosen ratio between photometrically derived and Balmer-ratio-derived extinction measures. The Calzetti value of $\gamma = 0.44$ is indicated as a long-dashed line. Right: percentage outliers for IMPZ (solid line with crosses) and HYPERZ (dot-dashed blue line, diamonds) as a function of γ. The Calzetti value of $\gamma = 0.44$ is indicated as a long-dashed line.
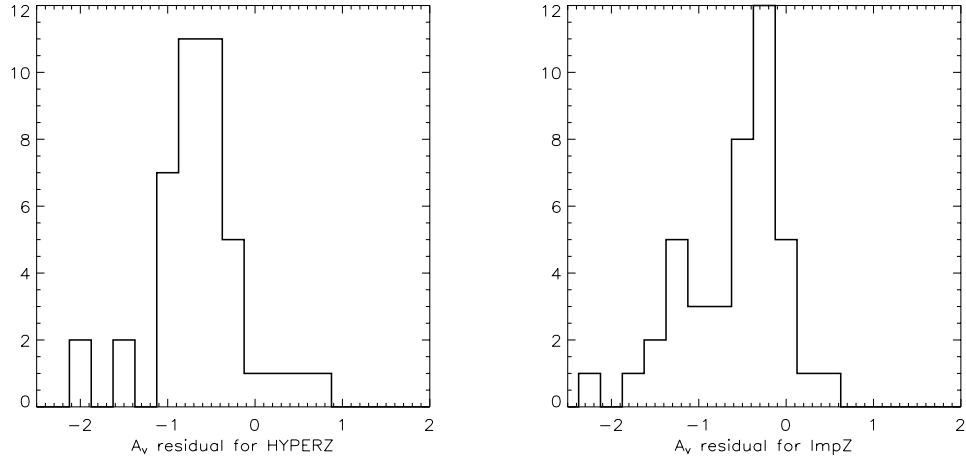
Figure 15. A_V residuals for HYPERZ (left) and IMPZ (right) with $\gamma = 0.25$. The residual is now $0.25 \times \text{Balmer}[A_V] - \text{Phot}[A_V]$.

Fig. 16 plots the Phot[A_V] values and residuals as a function of Balmer[A_V] (multiplied by $\gamma = 0.25$). It can be seen that, for lower Balmer[A_V], the Balmer[A_V] tends to underestimate the extinction compared with the Phot[A_V] value. If the negative Balmer[A_V] values are excluded, the remaining sources with positive Balmer[A_V] do tend to follow the line denoting agreement, albeit with large scatter.

In Fig. 17, the sources with only a lower limit on their Balmer-derived extinction (that is, a minimum 3σ Hα detection but a limit only on the Hβ line flux) are plotted in comparison with the extinction as derived from the photometric redshift codes. Here, no ratio γ is applied to the Balmer[A_V]. Instead, straight lines indicating different ratios are overplotted. Since these are lower limits, sources need to lie on, or to the left of, a line to imply consistency with that chosen ratio. It can be seen that these lower-limit sources are more consistent with lower values of γ. Of the 153 such sources, 146 (95 per cent) are consistent with the $\gamma = 0.25$ line when considering IMPZ solutions (purple squares), but only 130 (85 per cent) are consistent when considering the HYPERZ solutions (cyan triangles).

6 DISCUSSIONS AND CONCLUSIONS

A number of redshift codes routinely output an A_V value in addition to the best-fitting redshift, but little has been done to investigate the reliability and/or accuracy of such extinction measures. The main reason for this lies in the aim of such codes – they have been developed and optimized in order to derive *redshifts*. However, as the field of photometric redshift derivation matures, it is useful to consider some of the other parameters that redshift solutions produce.

In this paper we have asked whether a photometric redshift code can reliably determine dust extinction. The short answer would be: 'not to a great accuracy'.

Using a sample with extinctions derived from Balmer flux ratios, the A_V values produced by two photometric redshift codes, IMPZ and HYPERZ, have been compared with the Balmer[A_V] values.

First, it was demonstrated that the inclusion of A_V was crucial in order to obtain photometric redshifts of high accuracy and reliability, such that 95 per cent of the IMPZ results agreed with the spectroscopic redshifts to better than 0.1 in $\log(1 + z)$. Without the inclusion of A_V freedom, there was a systematic and incorrect offset
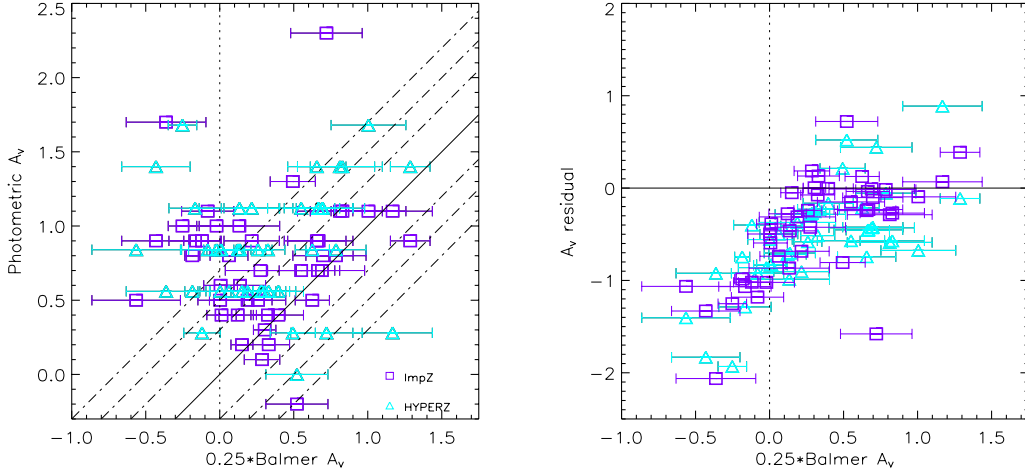
Figure 16. Left: A_V results for HYPERZ (cyan triangles) and IMPZ (purple squares). The plot is of the Balmer[A_V] (multiplied by $\gamma = 0.25$) versus the photometrically derived A_V. Dot-dashed lines denote residuals of 0.3, 0.5 and 0.7 in A_V. Errors are not defined for the Phot[A_V] values. Right: A_V residuals for HYPERZ (cyan triangles) and IMPZ (purple squares). The plot is of Balmer[A_V] (multiplied by $\gamma = 0.25$) versus the residual $0.25 \times$ Balmer[A_V]−Phot[A_V].
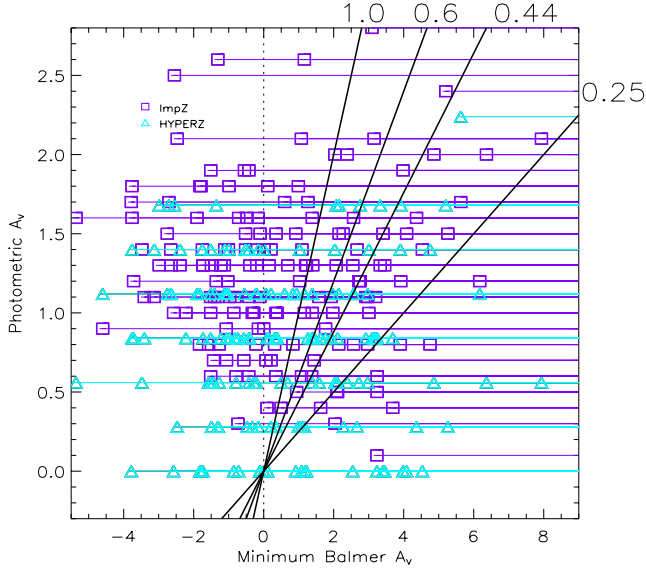
Figure 17. 'Limit' cases: A_V results for HYPERZ (cyan triangles) and IMPZ (purple squares). The plot is of the Balmer[A_V] 'limits' versus the photometrically derived A_V. Solid black lines denote γ values of 0.25, 0.44, 0.6 and 1.0 for the conversion factor relating Balmer[A_V] and Phot[A_V]. Sources need to lie on, or to the left of, a line to imply consistency with that chosen ratio.

to higher photometric redshifts, with many more incorrect redshift solutions. The existence of some negative A_V solutions may be indicative of the need for a bluer template in the template set, or for the inclusion of some additional free parameter in the fits. As the most important feature for template-fitted photometric redshifts is the location and identification of 'breaks' in the SED, the inclusion of A_V freedom can be seen, at first-order, as a modifier of the template SED's slope, but it does not have a strong effect on the breaks themselves. Hence a similar improvement may be achievable via a 'tilting' parameter, or similar, which would act to alter the slope of the template SEDs. Since the addition of dust extinction has a physical basis, however, this is a preferable parameter, as long as we can demonstrate that there is some correlation between the best-fitting Phot[A_V] and the actual (or in this case, that measured via

the Balmer ratio) dust extinction of the source. Thus, once the ability to derive good redshifts for the sample had been demonstrated a comparison between the Phot[A_V] and Balmer[A_V] was carried out.

The correlation between the Phot[A_V] and the Balmer[A_V] was similar for both codes, but was noisy and not particularly strong. Based on direct comparison between the two codes, and investigations into the χ^2 solution space, it was found that a good part of this noise is derived from the inherent lack of precision that the Phot[A_V] solution has (perhaps 0.3 in A_V say), no doubt since it is based on only five photometric measurements. Additional noise arises from the precision of the Balmer[A_V], typically accurate to perhaps 30 per cent, as a result of the resolution of the spectrographic data. Given these errors, the correlation seen was, in fact, quite good.

The correlation was improved somewhat when the empirical value of $\gamma = 0.44$, the ratio between gas- and star- derived extinction, as determined by Calzetti (2001b), was allowed to vary. From least-squares fitting, the minimum in the reduced χ^2 distribution was found for $\gamma \sim 0.25 \pm 0.2$.

The Calzetti ratio of 0.44 means that there is a factor of about 2 difference in reddening, such that the ionized gas (as measured by the Balmer decrement) is twice as reddened as the stellar continua (as measured by the photometry) (e.g. Fanelli, O'Connell & Thuan 1988; Calzetti et al. 1994). This implies that the covering factor of the dust is larger for the gas than for the stars, which can be explained by the fact that the ionizing stars are short-lived and so for their lifetime remain relatively close to their (dusty) birthplace, whilst the majority of stars contributing to the galaxy's overall optical luminosity are longer-lived and can migrate away from their dusty origins.

For the sample of galaxies in this paper, this factor of 2 difference in covering factor implied by the Calzetti ratio is found to be plausible, given the errors of the method. The sample has some preference for an increased covering factor, which implies that these galaxies are undergoing more rapid, 'bursty' star formation than the galaxies Calzetti used in her derivation. Perhaps more importantly, the results demonstrate the pitfalls of assuming that star- and gas-based extinction measures will give the same dust extinction given some conversion factor. Thus, correlation to Balmer-derived values are modulo the uncertainty in comparing star- and gas-based extinction measures.

However, the results presented here show that, given certain considerations, there is potential in the application of photometric codes to derive a reliable extinction measure, although the precision is currently low. It is expected that the ability of photometric redshift codes to determine extinction will improve with the availability of more photometric bands (here, there are five wide-band filters between 3000 and 9000 Å). A sample with a combination of wide- and narrow-band filters, with good wavelength coverage and range (in particular, extension to near-IR) will break many of the degeneracies and allow the codes to differentiate accurately between different possible fits.

The results also show that it is important to note that this will be a measure of the star-based extinction, and will not necessarily be well correlated with the extinction to the ionized regions of a galaxy.

ACKNOWLEDGMENTS

REFERENCES

Adelberger K., Steidel C., 2000, ApJ, 544, 218
Babbedge T. S. R. et al., 2004, MNRAS, 353, 654 (B04)
Balogh M., 1999, PhD thesis, Univ. Durham
Balogh M., Bower R. G., Smail I., Ziegler B. L., Davies R. L., Gaztelu A., Fritz A., 2002, MNRAS, 337, 256
Berta S., Fritz J., Franceschini A., Bressan A., Lonsdale C., 2004, A&A, 418, 913
Bohlin R., Jenkins E., Spitzer L., York D., Hill J., Savage B., Snow T., 1983, ApJS, 51, 277
Bolzonella M., Miralles J.-M., Pelló R., 2000, A&A, 363, 476
Bressan A., Granato G., Silva L., 1998, A&A, 332, 135
Calzetti D., 1997, astro-ph/9706121
Calzetti D., 2001a, PASP, 113, 1449
Calzetti D., 2001b, New Astron. Rev., 45, 601
Calzetti D., Heckman T., 1999, ApJ, 519, 27
Calzetti D., Kinney A., Storchi-Bergmann T., Panagia N., 1993, Bull. Am. Astron. Soc., 25, 841
Calzetti D., Kinney A., Storchi-Bergmann T., 1994, ApJ, 429, 582
Calzetti D., Kinney A., Storchi-Bergmann T., 1996, ApJ, 458, 132
Calzetti D., Armus L., Bohlin R., Kinney A., Koornneef J., Storchi-Bergmann T., 2000, ApJ, 533, 682
Cardelli J., Clayton G., Mathis J., 1989, ApJ, 345, 245
Carlberg R., Yee H., Morris S., Lin H., Hall P., Patton D., Sawicki M., Shepherd C., 2000, ApJ, 542, 57
Crampton D. et al., 1992, in Ulrich M. H., ed., Proc. ESO Conf. on Progress in Telescop and Instrumentation Technologies MOS/SIS Project. ESO, Garching, p. 609
Dressler A., Shectman S. A., 1987, AJ, 94, 899
Fanelli M., O'Connell R., Thuan T., 1988, ApJ, 334, 665
Ferland G., Korista K., Verner D., Ferguson J., Kingdon J., Verner E., 1998, PASP, 110, 761
Hauser M. et al., 1998, ApJ, 508, 25
Hopkins A. M. et al., 2003, ApJ, 599, 971
Kennicutt R., 1992, ApJ, 388, 310
Kennicutt R. C., Kent S. M., 1983, AJ, 88, 1094
Kewley L., Geller M., Jansen R., Dopita M., 2002, AJ, 124, 3135
Kurucz R., 1993, ATLAS9 Stellar Atmosphere Programs and 2 km s^{-1} Grid. Kurucz CD-ROM No.13. Smithsonian Astrophysical Observatory, Cambridge, MA
Madau P., Ferguson H., Dickinson M., Giavalisco M., Steidel C., Fruchter A., 1996, MNRAS, 283, 1388
Massarotti M., Iovino A., Buzzoni A., 2001, A&A, 368, 74
Meurer G., Heckman T., Calzetti D., 1999, ApJ, 521, 64
Miller N. A., Owen F. N., 2002, AJ, 124, 2453
Osterbrock D., 1989, Astrophysics of Gaseous Nebulae and Active Galactic Nuclei. University Science Books, Mill Valley, CA
Pettini M., Kellogg M., Steidel C., Dickinson M., Adelberger K., Giavalisco M., 1998, ApJ, 508, 539
Pickles A., 1998, PASP, 110, 863
Puget J. L., Abergel A., Bernard J. P., Boulanger F., Burton W. B., Desert F. X., Hartmann D., 1996, A&A, 308, L5
Rowan-Robinson M., 2003, MNRAS, 344, 13 (RR03)
Rowan-Robinson M. et al., 1997, MNRAS, 289, 490
Savage B., Mathis J., 1979, ARA&A, 17, 73
Shepherd C., Carlberg R., Yee H., Morris S., Lin H., Sawicki M., Hall P., Patton D., 2001, ApJ, 560, 72
Tody D., 1993, in Hanisch R. J., Brissenden R. J. V., Barnes J., eds, ASP Conf. Ser. Vol. 52, Astronomical Data Analysis Software and Systems II. Astron. Soc. Pac., San Francisco, p. 173
Westera P., Cuisinier F., Telles E., Kehrig C., 2004, A&A, 423, 133
Yee H. et al., 2000, ApJS, 129, 475

This paper has been typeset from a TeX/LaTeX file prepared by the author.